Journal of Catalysis 405 (2022) 614–625

Contents lists available at ScienceDirect

Journal of Catalysis

journal homepage: www.elsevier.com/locate/jcat

PERSPECTIVE

The Fischer-Tropsch synthesis: A few enduring mechanistic conundrums revisited

Enrique Iglesia [a,*], David Hibbitts [b]

[a] Department of Chemical Engineering, University of California at Berkeley, Berkeley, CA 94720, USA
[b] Department of Chemical Engineering, University of Florida, Gainesville, FL, 32611, USA

ARTICLE INFO

Article history:
Received 10 September 2021
Revised 26 October 2021
Accepted 27 October 2021
Available online 1 December 2021

Keywords:
Fischer-Tropsch synthesis
CO activation
C-C bond formation
Co-adsorbate interactions
Coverage effects

Few catalytic processes have garnered attention in practice as persistently as the Fischer-Tropsch synthesis (FTS); even fewer have led to the passionate mechanistic polemics that have characterized its storied history. Not many reactions have generated such diverse mechanistic proposals or faced the task of discerning among them from data often corrupted by ubiquitous gradients in temperatures and concentrations or by confounding matters of gas-liquid-solid interfaces. None have done so amidst active deployment in practice or through cycles of attention that fluctuate with remarkable regularity, as gas conversion technologies have responded to cyclical geopolitical disruptions, shifts in market demand, or unexpected discoveries of gas reservoirs, often remote from markets. These waves of interest have stranded mechanistic debris; each cycle has faced the inconvenient truths, enduring inconsistencies, and mechanistic proposals of those before.

This Perspective puts forth concepts and tenets that, in our view, resolve mechanistic puzzles that have persisted throughout the history of FTS: (i) how is bound CO (CO*) activated if its dissociation requires very large barriers on the low-index surfaces that prevail on the most active Co and Ru particles; (ii) how does CO* dissociate when landing spaces are so scarce within dense adlayers of strongly bound CO*; (iii) why does water enhance turnover rates and the predominance of longer chains; and (iv) how can chains grow fast and long if monomers form throughout dense CO* adlayers that inhibit monomer diffusion? These mechanistic conundrums are not new; yet they are often ignored or explained by elaborate constructs or contrived site architectures that were discarded in previous cycles. This Perspective focuses on Co and Ru, which are the catalysts of choice for the synthesis of long paraffinic chains at low temperatures. Such catalysts are also best suited for benchmarking theory and experiment because Fe-based catalysts require textural and chemical promoters and undergo chemical and structural oxide-carbide-metal interconversions during FTS.

Recent advances in theory and experiment lead us now to consider how densely covered nanoparticles can create environments that enable kinetic channels inaccessible on sparsely covered flat surfaces, which have served us well as learning models of the more complex realities of catalysis practice. Reaction-transport formalisms allow us to assess (and often to eliminate) transport corruptions of measured rates and selectivities and to describe important details of the product chain length and degree of unsaturation [1]. Emerging theoretical methods can now describe curved nanoparticle surfaces at relevant CO* coverages and assess with unprecedented fidelity the identity and relevance of elementary steps, intermediates, and site architectures. Our cherished Langmuirian treatments of surface reactions had to be reconsidered in spite of their remarkable success in describing the effects of reactant and product concentrations on rates and selectivities;

* Corresponding author.
E-mail address: iglesia@berkeley.edu (E. Iglesia).

https://doi.org/10.1016/j.jcat.2021.10.033
0021-9517/

non-Langmuirian surface reaction models then served to reconcile the prevalent discrepancies between CO* coverages from in situ infrared spectra and those inferred from Langmuirian kinetic models.

This Perspective describes work spanning more than three decades and the efforts and talents of many with whom we have labored on FTS matters. These include students and post-doctoral researchers,[1] academic colleagues (M. Neurock, M. Mavrikakis), and coworkers[2] in the practical trenches of gas conversion technologies. The work has evolved through many cycles; each cycle harvested the knowledge and the puzzles, through new tools and concepts, but also the clarity that emerged from our previous work and that of others. Now, encouraged by fewer obvious contradictions, we address the enduring mechanistic puzzles that emerged and were resolved throughout these cycles, all in the spirit of finding those new ones that we do not yet know of.

The earliest FTS mechanism by Fischer and Tropsch involved hydrocarbons formed via reactions of carbide moieties with H_2 [2]; yet, such metal carbides form only CH_4 upon contact with H_2 [3]. Alternate early proposals were frequently informed by analogies with catalysis by organometallic complexes [4,5]. Storch and Goulombic proposed that C—C bonds formed via condensation of enols bound through their C-atom (HC*OH) [5]. Carbene-mediated routes envisioned CO* dissociation to C* and O* and C* reactions with H* to form M = CH_2* species (M: metal) that added to growing chains [6–9]. CO* itself has been proposed as the monomer, with C—C bonds formed via alkyl migration, as in carbonylation reactions on organometallic complexes [10–14].

The facile CO* activation steps required to account for fast FTS turnovers led to proposed site architectures, often involving defects that grew increasingly complex as simpler constructs failed to account for measured rates or activation barriers. These architectures were inspired by observations of facile direct CO* dissociation events at low-coordination atoms on extended surfaces and by density functional theory (DFT) studies of stoichiometric CO reactions on sparsely covered surfaces. Specific step-edge sites (known as B5 sites) can enable facile CO* activation via η^2-binding through concerted C—M and O—M bond formation [15], in contrast with high-barrier routes involving $\eta 1$-binding (M—CO) on edges, corners, or low-index planes [16–19]. The higher FTS turnover rates measured on low-index facets of Co and Ru, which lack indigenous B5 sites, were attributed to surface "roughening" induced by bound CO*; such roughening occurs on some extended flat surfaces upon CO binding [20–22] and even on certain dispersed Pt nanoparticles, on which specific CO* infrared features emerge bands upon extended contact with CO [23]. These features have not been detected on dispersed Co or Ru nanoparticles during H_2-CO reactions, even at the high CO pressures and coverages prevalent during FTS [16,17,24,25]. These defect sites, if present on small particles, bind CO* and its dissociation products strongly, thus precluding turnovers, as discussed below; their kinetic irrelevance may account for the low turnover rates measured on small Co [18,26] and Ru [15,27,28] particles.

The heuristic constructs brought into FTS catalysis from seemingly adjacent chemistries did not consider, at least as first proposed, that: (i) mononuclear organometallic complexes do not contain contiguous metal atoms, thus requiring singly bound CH_2* and CO* as monomers for C—C bond formation in such models; (ii) open coordination sites, needed for binding and activation, require that strongly bound CO* desorb from dense CO* adlayers; (iii) coadsorbed ligands, and specifically H*, can assist C—O cleavage, thus circumventing the need for adlayer vacancies (*) in direct CO* dissociation events; and (iv) the low coverages present in theoretical and high-vacuum studies cannot describe the ubiquitous effects of site-blocking by unreactive fragments from direct CO* dissociation or the coadsorbate interactions that dictate reactivity and which, in fact, make FTS catalytic turnovers at all possible.

The formation of long chains in FTS requires high pressures and occurs in dense CO* adlayers at nanoparticle surfaces that reside within pores filled with liquid hydrocarbons, which impose diffusional hurdles that obstruct direct measurements of the dynamics and selectivities of surface-catalyzed events and their mechanistic interpretation. These complex environments also pose formidable challenges to spectroscopic inquiries and to theoretical treatments of reactions on the curved and crowded surfaces of Co and Ru nanoparticles. Such challenges are often "bypassed" by using flat model surfaces and low pressures or by studying the binding of CO without H_2 coreactants; these approaches make these systems amenable to spectroscopic and theoretical tools, but they fail to account for why FTS turnovers prefer low-index surface planes, why few chains grow long and fast within CO* adlayers that obstruct monomer migration, or even how CO* reacts at all, given its strong binding and unreactive nature on sparsely-covered surfaces. These conundrums reflect the use of a Langmuirian canon appropriate for model surfaces at low coverages, but which becomes inaccurate on curved and crowded surfaces. In fact, crowded surfaces allow coadsorbed species to assist the activation of bound molecules with strong bonds [29] and weaken their binding, thus enabling the presence of "spaces" to bind coreactants. Dense adlayers are locally disrupted by growing chains, thus creating "spaces" to stabilize transition states for the formation of CH* monomers precisely where such monomers are required to grow chains.

Such considerations resolve, in our view and based on theory and experiments at the realistic conditions of crowded surfaces, four of these conundrums. Yet, this is our Perspective; we expect that it will contrast the views of others, with the intensity that our discipline reserves for polemics about FTS mechanisms. The concepts and treatments underpinning an analysis of FTS catalysis represent recyclable knowledge beyond our current intent. We have structured this Perspective as a sequence of these mechanistic puzzles; they are resolved using a robust framework that considers how crowded surfaces, difficult to assess by experiment or theory, mediate (and are essential for) catalytic turnovers of strongly bound intermediates.

The recent advances in addressing these puzzles have benefited from combined kinetic, spectroscopic, and theoretical methods used to probe the elementary steps and sites involved in forming monomers and C—C bonds on Ru and Co catalysts to address how:

(i) FTS turnovers occur on surfaces covered by dense CO* adlayers and with few bare sites accessible for direct CO* dissociation.
(ii) the high-barrier direct CO* dissociation routes on bare low-index planes are circumvented by routes assisted by the sequential addition of H* to the C and O atoms in CO* (to form *HCOH*), thus weakening C—O bonds before cleavage forms CH* and OH*.
(iii) CO* adlayers densify as CO pressure increases, leading to the preferential destabilization of CO* relative to the smaller H-assisted CO* dissociation transition states, thus decreasing activation barriers.
(iv) H_2O, a FTS product, increases turnover rates and chain growth selectivities via proton-coupled electron transfer processes that decrease H-assisted CO activation barriers, thus increasing CH* monomer formation rates.

[*] M. Ojeda, S. Krishnamoorthy, B. Loveless, C. Buda, E. Dybeck, J. Liu, A. Li, R. Nabar, A. Nilekar, S. Li, G. Meitzner.
[2] S. C. Reyes, S. L. Soled, S. Miseo, ExxonMobil.

(v) a few chains grow very fast because chains locally disrupt CO* adlayers, thus making "space" for *HCOH* and CH* formation, thus avoiding the need for endothermic CO* desorption and for CH* migration through dense adlayers.

1. FTS occurs in practice on curved and crowded nanoparticles

On Co and Ru, FTS turnover rates are inhibited by CO and can be accurately described by:

$$r_{CO} = \frac{\alpha P_{H_2} P_{CO}}{(1 + \beta P_{CO})^2} \quad (1)$$

albeit with α and β values that differ in chemical origins and magnitude for different mechanistic interpretations [16,30–33]. Such Langmuirian equations seem incompatible with the high CO* coverages prevalent during FTS practice, as do the β values derived from Eq. (1), which are significantly smaller than CO adsorption constants measured directly from infrared spectra during FTS reactions [24].

The CO inhibition demonstrated in Eq. (1) is consistent with the strong CO* infrared bands evident during H_2-CO reactions on Co and Ru nanoparticles. Their intensity becomes essentially independent of CO pressures even at higher temperatures and lower CO pressures than those used in FTS reactions (500–600 K; 10^{-3}–10 kPa CO; 5 wt. % Ru/SiO_2, 7.5 nm mean diameter, Fig. 1c). These infrared bands grow in the manner expected from Langmuir adsorption below 1 kPa CO, but their intensity continues to increase gradually (and bands shift slightly to higher frequencies) at higher pressures, indicative of a gradual densification of CO* adlayers that leads to stronger dipole–dipole interactions, to the binding of multiple CO* at low-coordination Ru atoms [34-–37], and to non-Langmuirian adsorption and kinetic behaviors. Specifically, CO adsorption equilibrium constants derived from such spectra decrease with increasing CO* coverage (Section 2). Similar experiments on Co nanoparticles led to identical conclusions [25]. The single band for atop CO* on Co nanoparticles (~10 nm mean diameter; 10 wt. % Co/SiO_2) shifts from 1960 to 2000 cm^{-1} as CO pressure increases (10^{-3}–10 kPa CO, 60 kPa H_2, 548 K) and the band intensities exhibit Langmuirian behavior only up to ~1 kPa CO and then increase very gradually (1–10 kPa CO) [25]. These data show that Co and Ru surfaces are saturated with dense CO* adlayers even at CO pressures 10–100 times lower than those required for FTS catalysis in practice.

CO* coverages (as ML, CO^*/M_{surf}) near unity are not achievable on flat extended surfaces (e.g., Ru(0001) [38], Co(0001) [39]); such model surfaces enable precise descriptions of bound species by experiment and theory, but without H_2 coreactants, organic and H_2O products, or the occurrence of catalytic turnovers. DFT-derived treatments show that the formation of a CO* adlayer is endothermic (with a differential binding energy of +16 kJ mol^{-1} to form a 1 ML surface) on Ru(0001), suggesting that saturation would occur at about 2/3 ML CO*, in agreement with measured CO coverages on Ru(0001) single crystals [16,38,40]. These extended flat surfaces prevent lateral relaxation of CO* adlayers to dampen intermolecular repulsion, in contrast with curved nanoparticle surfaces; single crystals and foils can relax only via atomic displacements perpendicular to the surface, leading to corrugated surfaces [41,42] that are indigenous for nanoparticles.

DFT-derived geometries indicate that Ru-Ru distances at nanoparticle surfaces increase with increasing CO* coverage and that linear CO* species 'fan out', thus minimizing intermolecular repulsion via processes unavailable for extended surfaces. On Ru_{201} nanoparticles (201 atoms), CO* adsorption remains quite exothermic at 1 ML CO* (−108 kJ mol^{-1} vs. + 16 kJ mol^{-1} on Ru(0001)); its binding enthalpy remains negative even at 1.05 ML CO* [16]. These large discrepancies have also been reported in DFT treatments of CO* adsorption on Ru_{57} hcp clusters [43] and larger Ru_{201} nanoparticles [16,44], and for NO* species on Rh_{201} [45], H* adsorption on Pt_{38-586} and Ir_{38-586} [46,47], and S* adsorption on Re_{201}, Ru_{201}, and Pt_{201} nanoparticles [48]. Extended surfaces are essential for theory–experiment benchmarking and to validate DFT treatments [49,50]; reliable descriptions of FTS dynamics require, however, that binding and reactivity descriptions be extended to curved and inherently non-uniform nanoparticle surfaces at CO* coverages prevalent during FTS [16,44,45,47].

2. CO activation is assisted by chemisorbed H atoms

Direct CO* dissociation at low-index Co and Ru surfaces:

$$CO^* + * \rightarrow C^* + O^* \quad \text{Rxn.(1)}$$

requires high activation barriers (>200 kJ mol^{-1} [16,51]). A sequence mediated by direct CO* dissociation (Rxn. (1)) on CO*-saturated surfaces would give FTS turnover rates:

$$r_{CO} = \frac{k_1}{K_{CO} P_{CO}} \quad (2)$$

with K_{CO} as the equilibrium CO adsorption constant and k_1 as the rate constant for CO* dissociation (Rxn. (1)); this equation is inconsistent with measured effects of H_2 on rates (Eq. (1)) [16,30-33]. The resulting rate constant ($k_{app} = k_1/K_{CO}$) would give apparent barriers:

$$\Delta E_{app} = \Delta E_{act,1} - \Delta E_{ads,CO} \quad (3)$$

that reflect the combined energies for CO* activation ($\Delta E_{act,1}$) and CO* desorption ($-\Delta E_{ads,CO}$). DFT-derived barriers for direct CO* dissociation ($\Delta E_{act,1}$) are 230 kJ mol^{-1} on low-index Co(0001) [19] and 227 kJ mol^{-1} on Ru(0001) [51] surfaces at modest coverages (≤0.5 ML CO*), which are much larger than measured barriers (~100 kJ mol^{-1}) [5,33,52-54]. FTS turnovers mediated by direct CO* dissociation would require the involvement of low-coordination step-edge sites, which have lower DFT-derived barriers for CO* dissociation on stepped surfaces of Co (68–136 kJ mol^{-1}) and Ru (47–89 kJ mol^{-1}) at modest coverages (≤0.5 ML CO*) [19,51,55]. Step-edge B5 sites at Ru(10 9) surfaces form stable C* atoms that titrate CO* binding sites [56], consistent with their reactivity in stoichiometric CO* dissociation but also with their incompetence in catalytic turnovers, a result of their irreversible poisoning by unreactive C* (and O*) dissociation products. These low barriers for CO* dissociation reported in literature fail to account for the essential requirement to create space for dissociation through CO* desorption events from densely covered surfaces and step-edge sites. This desorption energy explicitly appears in the apparent activation barrier (Eq. (3)).

On curved Ru_{201} nanoparticles (1.05 ML CO*), activation barriers (potential energies, $\Delta E_{act,1}$ in Eq. (3)) for unassisted CO* dissociation at a step-edge site are 150 kJ mol^{-1}; the energy required to desorb CO* from that step-edge site is 119 kJ mol^{-1} ($\Delta E_{ads,CO}$), leading to an appar-

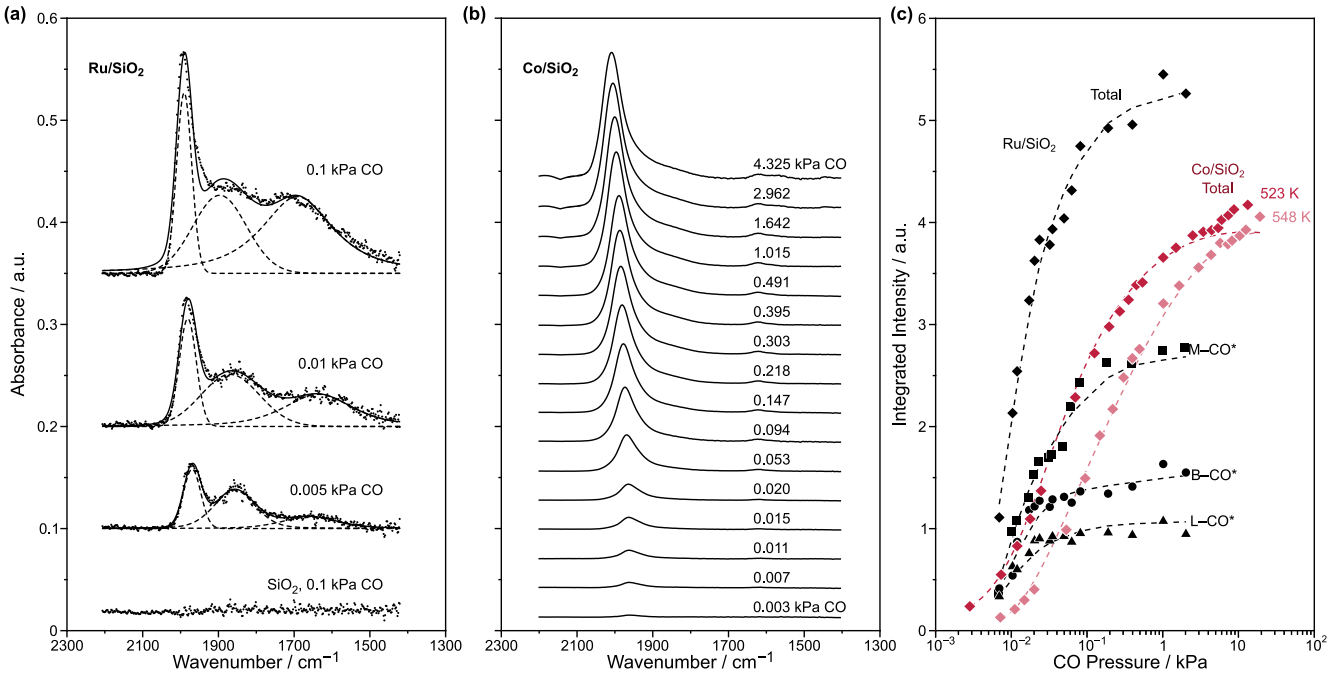

Fig. 1. (a) Infrared spectra during steady-state CO-H_2 reactions on SiO_2, 5 wt. % Ru/SiO_2 (0.005–0.1 kPa CO, 0.1–2 kPa H_2, balance He, 573 K) [24] and (b) on 10 wt. % Co/SiO_2 (0.003–4.3 kPa CO, 60 kPa H_2, balance He, 548 K) [25]. (c) Integrated intensities of C—O stretch bands for deconvoluted infrared spectra on Ru/SiO_2 (573 K) [24] and Co/SiO_2 (523–548 K) [25] as a function of CO* pressure (L-CO* for linear CO*, B-CO* for bridging CO*, M−CO* for CO* interacting with > 2 Ru surface atoms) and for L-CO* on Co/SiO_2.

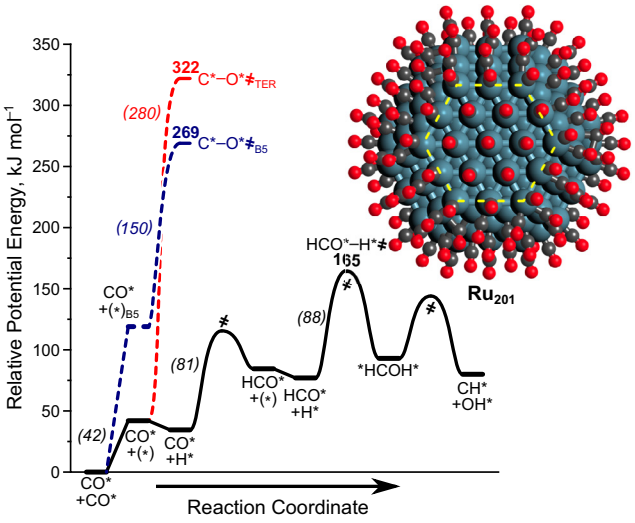

Fig. 2. DFT-derived potential energy surfaces (0 K, without zero-point vibrational energies) for CO* activation via direct dissociation on the (1 1 1) terrace (red, dashed), on step-edge (B5) sites (blue, dashed), and via H-assisted CO* activation (black) on (1 1 1) terrace sites [16]. Effective activation barriers (in bold) represent the energies to form the transition states from a CO*-covered surface, intrinsic barriers are denoted in italic print. The Ru_{201} model (inset) used to model these reactions is shown with the (1 1 1) terrace outlined in yellow.

ent barrier (269 kJ mol^{-1}; Eq. (3), Fig. 2) much larger than measured barriers (~100 kJ mol^{-1}). These sites dissociate CO* with lower apparent barriers than low-index planes on Ru_{201} nanoparticles (322 kJ mol^{-1}; Fig. 2), but direct CO* dissociation at either site cannot account for FTS turnovers. FTS catalytic sequences mediated by kinetically relevant direct CO* dissociation steps also cannot account for the effects of H_2 pressure on rates (Eq. (1)) unless such steps are quasi-equilibrated during FTS catalysis; such a scenario is rendered implausible (in spite of inferences from isotopic exchange data [57]) because of the strong binding of C* and O* at step-edge sites competent for direct dissociation and the high barriers for C*-O* recombination and CO desorption at such sites.

Strong bonds, such as those in CO, typically required sequential reactions of each atom in such bonds with coadsorbed species, instead of additional attachments of such atoms with exposed surface atoms; this becomes singularly essential on the densely covered surfaces ubiquitous in the practice of catalysis [29]. This represents the essence of catalysis at work: the replacement of difficult steps by a sequence of switchbacks in multi-dimensional energy space. Coadsorbate-assisted pathways are evident in O_2-H_2 (or O_2-H_2O) reactions on Au and Pd [58-61], NO-H_2 reactions on Pt and Rh [45,62], and CO-O_2 reactions on Au [61] and Pt [34]. In FTS, such routes take the form of CO* dissociation after sequential reactions with H*:

$$CO^* + H^* \leftrightarrow HCO^* \quad \text{Rxn.(2)}$$

$$HCO^* + H^* \rightarrow {}^*HCOH^* \quad \text{Rxn.(3)}$$

$$^*HCOH^* \rightarrow CH^* + OH^* \quad \text{Rxn.(4)}$$

in steps that weaken C—O bonds before cleavage [63-65]. In this sequence, Rxn. (2) is quasi-equilibrated and Rxns. (3) or (4) are kinetically relevant, a choice that leads to the same rate equation and which only theory can discern. The rate equation when Rxn. (3) limits FTS rates agrees with the form observed on Co and Ru catalysts [16,30-33] (Eq. (1)):

$$r_{CO} = \frac{k_3 K_2 K_{H_2} K_{CO} P_{H_2} P_{CO}}{(1 + K_{CO} P_{CO})^2} \quad (4)$$

with K_2 and k_3 as equilibrium and rate constants and K_{CO} and K_{H_2} as equilibrium constants for CO adsorption and dissociative H_2 adsorption, respectively. On nearly saturated surfaces ($K_{CO}P_{CO} \gg 1$), rates become:

$$r_{CO} = \frac{k_3 K_2 K_{H_2} P_{H_2}}{K_{CO} P_{CO}} \quad (5)$$

The lumped rate constant:

$$k_{app} = k_3 K_2 K_{H_2} / K_{CO} \quad (6)$$

reflects an apparent barrier:

$$\Delta E_{app} = \Delta E_{act,3} + \Delta E_{rxn,2} + \Delta E_{ads,H_2} - \Delta E_{ads,CO} \quad (7)$$

with terms that can be determined from DFT-derived activation barriers (E_{act}) and reaction energies (E_{rxn}) for each step and adsorption energies (E_{ads}) for each bound reactant. On Ru_{201} terraces, the DFT-derived apparent barrier for the lumped rate constant is 165 kJ mol^{-1}, compared to 269 kJ mol^{-1} for direct CO* dissociation on B5 step-edge sites and 322 kJ mol^{-1} for direct dissociation on low-index terraces [16]. An earlier study on Co(0001) surfaces with 0.5 ML CO* also concluded that H-assisted CO* routes give barriers that are much smaller (by 192 kJ mol^{-1}) than for direct CO* dissociation [30,66]. CO cleavage is preceded by sequential weakening of C—O bonds via reactions with H*; activation barriers are much smaller than for direct dissociation even on low-coordination step-edge sites; these specific site architectures are inconsistent with FTS turnovers that are favored on large Co and Ru nanoparticles that predominantly expose low-index planes [18,31,32].

H-assisted pathways account for the competence of low-index planes in CO* activation, without requiring surface structures that are not indigenous on the low-index planes prevalent on large Co and Ru nanoparticles. Such assisted routes provide yet another illustration of how surfaces dissect bond-breaking into a larger number of less challenging steps; the use of H* in this case parallels how assistance is involved in NO* activation (via *HNOH*) [45,62] and O_2* activation in O_2-H_2 and O_2-H_2O reactions (via *OOH*) [58-61]. These processes find few analogies in organometallic catalysts because their low nuclearity disfavors coadsorbate interactions and bimolecular encounters; they are ubiquitous, however, in catalysis on crowded surfaces.

H-assisted CO* activation routes have become the accepted paradigm through theoretical and experimental confirmations since first proposed [67-72]; deliberations persist only about the kinetic relevance of the first (Rxn. (2)) or second (Rxn. (3)) sequential H-addition and about residual attachments to B5 sites, even though their emergence to account for the incompetence of low-index planes in direct CO* activation is rendered unnecessary by bimolecular assisted routes. Nevertheless, some of the imperatives made evident from these conclusions are inconvenient—that curved and crowded surfaces prevail in practice and that flat surfaces (even at moderate coverages) in the absence of coreactants or catalytic turnovers cannot provide evidence for the competence of bimolecular routes. To some extent, the resulting recalcitrance to accept such evidence may reflect how DFT-derived activation barriers for H-assisted CO* activation events still remain somewhat larger than measured barriers, even at supra-monolayer CO* coverages (165 kJ mol^{-1} at 1.05 ML CO* vs. ~100 kJ mol^{-1}) [5,33,52-54].

These remaining differences reflect, at least in part, (i) the inadequacy of Langmuirian models in describing reaction rates within dense liquid-like CO* adlayers [24]; (ii) the role of H_2O in enhancing rates and chain growth [73]; and (iii) the observation that H-assisted CO* activation becomes even more facile near chains, as they disrupt the dense CO* adlayers [44]. These effects cause H-assisted CO* activation barriers to become even smaller, as discussed next.

3. CO* adlayers densify as CO pressures increase leading to lower barriers through preferential destabilization of adlayers over *HCO–H*≠ transition states

Low-coordination "defect" sites are titrated by unreactive CO* or its C*/O* dissociation products, but weaker-binding low-index terraces become kinetically competent with bimolecular H-assistance in dense CO* adlayers that cover nanoparticle surfaces during FTS. These dense adlayers lack open sites for binding direct CO* dissociation transition states, but also weaken CO* binding through CO*–CO* repulsion, thus precluding Langmuirian kinetic treatments and requiring that DFT-derived binding energies and activation barriers be calculated at the supramonolayer CO* coverages that prevail on nanoparticles but not on extended surfaces. The success of Langmuirian rate equations (Eqs. (1), (4)) in describing rate data is fortuitous, as evident from kinetic and thermodynamic parameters regressed from the rate data using such equations.

At low CO pressures (0.01–1 kPa CO), K_{CO} values regressed from rate data and Eq. (4) on Ru/SiO_2 are similar to those derived from Langmuirian descriptions of infrared CO* band intensities during reaction (Fig. 3; 518–598 K), as expected at the prevalent submonolayer CO* coverages [24]. At higher CO pressures (10–100 kPa CO), K_{CO} values from rate data are ~100-times smaller than measured from rate or infrared data at lower pressures (Fig. 3), even though rates can be accurately described by Eq. (4) in this pressure range (10–100 kPa

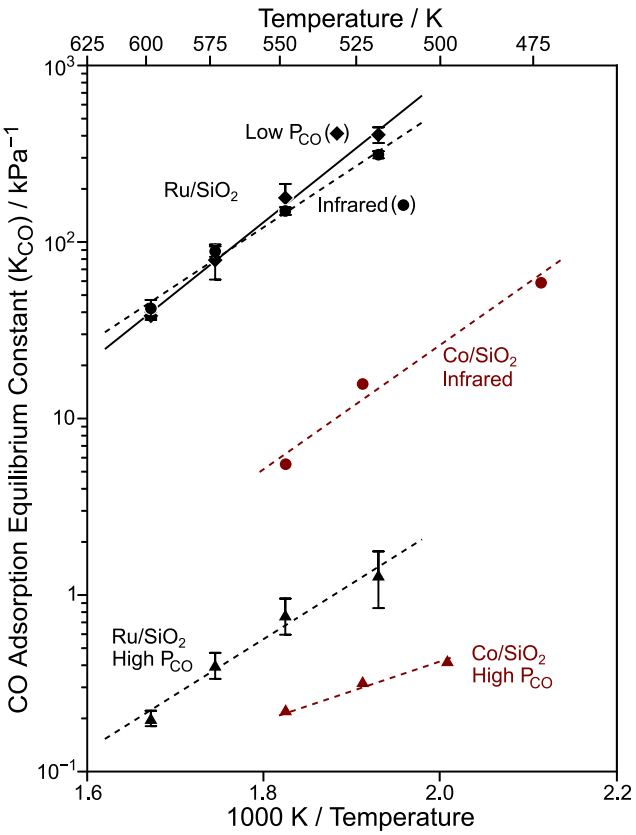

Fig. 3. Regressed CO adsorption constants (K_{CO}) from IR data (●), low-pressure rate data (10^{-3}–10^{-1} kPa CO, ◆), and high-pressure rate data (10–100 kPa CO, ▲) on Ru/SiO_2 at 518–598 K [24] and on Co/SiO_2 at 473–548 K [25].

CO, 518–598 K). Higher CO* coverages and stronger CO*–CO* repulsion cause CO* binding energies and K_{CO} values to decrease when CO* adlayers densify as CO pressures approach those prevalent in FTS reactions (0.1–1 MPa CO; 450–550 K). These very different K_{CO} values at high and low CO pressures are also evident on Co-based catalysts (10 wt% Co/SiO_2) [25]; K_{CO} values from infrared CO* bands at submonolayer coverages (0.01–1 kPa CO, 473–548 K) are ~50 times larger than those derived from CO pressure effects on FTS rates described by Eq. (4) at higher CO pressures (4–12 kPa; Fig. 3).

The effects of CO* coverages on K_{CO} as CO* coverages approach saturation cause a monotonic increase in k_{app} (Eq. (6)) with CO pressure and lead to CO pressure effects on rates that mimic the presence of both terms in the denominator of Eq. (4). In fact, K_{CO} cannot be independently determined from rates at near-monolayer coverages, indicating that Eq. (4) is an inaccurate description of FTS rates. Instead, Eq. (5) can be used and proves useful, because the apparent rate parameter (k_{app}, Eq. (6)) increases monotonically with increasing CO pressure and thus with CO* coverages.

The magnitude of k_{app} (Eq. (6)) depends on the free energy of formation of the kinetically relevant *HCO–H*‡ transition state (TS) from two bound CO* molecules and one H_2(g):

$$k_{app} = \frac{k_3 K_2 K_{H_2}}{K_{CO}} = \frac{k_B T}{h} K^{\ddagger} = \frac{k_B T}{h} e^{\left(\frac{-\Delta G^{\ddagger}}{RT}\right)} \tag{8}$$

with an equilibrium constant ($K^{\ddagger}$) and an apparent free energy barrier ($\Delta G^{\ddagger}$). $K^{\ddagger}$ (and $\Delta G^{\ddagger}$) values are those for the formation of the TS in a lumped chemical event described as:

$$2\ CO^* + H_2(g) \overset{K^{\ddagger}}{\leftrightarrow} {}^*HCO\text{–}H^{*\ddagger} + CO(g) \qquad \text{Rxn.(5)}$$

a stoichiometry that reflects the need to remove two CO* to form the bidentate TS. The $\Delta G^{\ddagger}$ for this reaction:

$$\Delta G^{\ddagger} = G[\,{}^*HCO\text{–}H^{*\ddagger}\,] + G[CO(g)] - G[2\ CO^*] - G[H_2(g)] \tag{9}$$

provides the theoretical underpinning required to assess how k_{app} varies with CO* coverage.

The *HCO–H* formation TS occupies a smaller area (0.1217 nm^2) than the two CO* molecules that must desorb to accommodate it (0.1574 nm^2) (DFT-derived structures; Ru_{218} clusters; 1.04 ML CO* [24]). The "activation area" ($\Delta A^{\ddagger}$; by analogy with activation volumes for reactions within a fluid phase [74-78]) for the reaction in Rxn. (5) is negative. In two-dimensions, negative activation areas cause apparent rate constants (k_{app}) to increase as the CO* coverage (and thus surface tension, τ) increases:

$$\frac{\partial \ln k_{app}}{\partial \tau} = -\Delta A^{\ddagger} \tag{10}$$

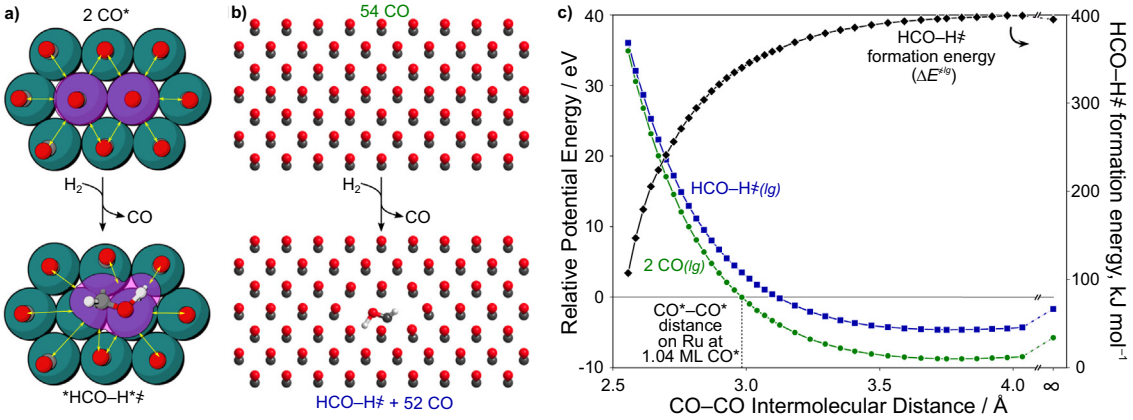

Fig. 4. (a) CO* pairs on the catalyst surface react with H_2 to form gas-phase CO and the *HCO–H*≠ transition state that activates CO* (Rxn. (5)). (b) This same reaction to form the HCO–H≠ transition state (Rxn. (5)) modeled here within a hexagonal lattice gas model of 54 total CO. (c) Change in potential energies (relative to a hexagonal CO lattice (part b) with an intermolecular distance of 2.97 Å) for 2 CO (green) and the HCO–H≠ structure (blue) as a function of intermolecular CO distances. The HCO–H≠ transition state formation energy on this metal-free lattice gas model ($\Delta E^{\neq lg}$) is shown on the right-hand axis.

just as rate constants for homogeneous systems with negative activation volumes ($\Delta V^{\neq}$) increase with increasing fluid pressure [75,77]. The surface tension term (τ) reflects coadsorbate repulsion at the contact boundary between the TS (or CO*) and the surrounding dense CO* adlayer; such repulsion is stronger as CO* coverage increases for both CO* and the TS, but to different extents.

These repulsive interactions destabilize larger structures (CO*–CO* pairs) more strongly than the smaller *HCO–H* formation TS as CO* adlayers densify. DFT treatments cannot capture monotonic changes in CO* coverage because of the inherent symmetry of extended surfaces and nanoparticle models, thus precluding calculations that vary CO* coverages with the required granularity. The promiscuous binding of CO* on metals (atop, bridge, three-fold), evident from theory and infrared spectra indicate, however, that through-space CO*–CO* repulsive effects are significant; consequently, adlayer densification effects can be captured directionally by lattice models that pre-position CO* in close-packed configurations, without explicit descriptions of surface binding, in the form of two-dimensional lattice gas models (Fig. 4b).

The uniform compression of this lattice gas decreases CO*–CO* distances, thus mimicking the monotonic densification of CO* adlayers in practice. A smaller mean CO*–CO* distance leads to higher energies for CO*–CO* pairs and the *HCO–H* formation TS (Fig. 4c), but such destabilization is less pronounced for the TS than the CO*–CO* pairs. These different sensitivities of the CO*–CO* pair and HCO–H* formation TS to the CO* adlayer density cause activation barriers to decrease from ~400 kJ mol^{-1} at essentially non-interacting CO*–CO* distances (~0.4 nm) to ~340 kJ mol^{-1} at the CO*–CO* distances for 1.05 ML on Ru_{201} terraces and to continue to decrease at shorter CO*–CO* distances. Of course, such high barriers (>300 kJ mol^{-1}) reflect the absence of the catalyst in this lattice gas model, but the trends parallel those for $\Delta G^{\neq}$ (548 K, Eq. (9)) on Ru_{201} models, which decrease from 280 kJ mol^{-1} on essentially bare Ru_{201} particles (0.02 ML CO*) to 236 kJ mol^{-1} at 1 ML CO* and to 229 kJ mol^{-1} at 1.04 ML CO*. At higher coverages, these activation free energies would approach measured values. Taken together with the ubiquitous role of H_2O as a cocatalyst and of growing chains as "spacers" that promote local CO* activation (discussed below), these effects of CO* coverage bring theoretical predictions closer to the reactivity of the crowded non-ideal surfaces of Ru and Co nanoparticles.

FTS rates decrease as CO pressure increases, but less sensitively than inferred from Eq. (5) at near-saturation coverages, because $\Delta G^{\neq}$ decreases (and k_{app} increases) as denser CO* adlayers preferentially destabilize the CO* molecules removed to accommodate the *HCO–H* TS. The monotonic changes in k_{app} and K_{CO} because of adlayer densification allow Langmuirian treatments to describe measured rates, but by invoking K_{CO} values that could not have been measured from rate data at coverages near CO* saturation. These K_{CO} values (1.2 at 518 K and 0.2 at 598 K, Ru/SiO_2) are about 10^4 times smaller than those derived from infrared spectra at submonolayer coverages (0.01–1 kPa CO; Fig. 3) [24].

The dense and liquid-like nature of CO* adlayers breaches the limits of convenient Langmuirian descriptions but enable CO* dissociation to occur via bimolecular H-assisted pathways on low-index surfaces that are ineffective for direct CO* dissociation. Coadsorbed CO* and H* species are essential in CO* dissociation, as is H_2O (a ubiquitous FTS product) and the growing chains that locally disrupt CO* adlayers.

4. H_2O mediates H-transfer events and enhances H-assisted CO* activation rates

Water, whether as an indigenous FTS product or added to CO-H_2 coreactants, can increase FTS rates on some catalysts [17,31,79-82], but does not influence and even decreases rates on others [33,83-86]. On most Co and Ru catalysts, H_2O increases chain growth probabilities [17,31,79,80,83,87,88], causing a monotonic increase in the molecular weight and degree of unsaturation in products with increasing H_2O pressure.

These different effects on rates partly reflect competing contributions by inhibition through coadsorption of H_2O-derived species and rate enhancements, leading to maximum rates at intermediate H_2O pressures. The mechanism responsible for rate enhancements remained uncertain until H-assisted CO* activation pathways connected these H_2O effects with H-addition steps that can be mediated by H_2O through proton-coupled electron transfer [73]. The effects of support pore size on these H_2O-induced rate enhancements led to inferences about the plausible presence of intrapore aqueous or biphasic intrapore structures stabilized by FTS products acting as surfactants; such intrapore liquids may create local environments that enhance or inhibit diffusion rates, with consequences for turnover rates and selectivities [1,17,85,89-91].

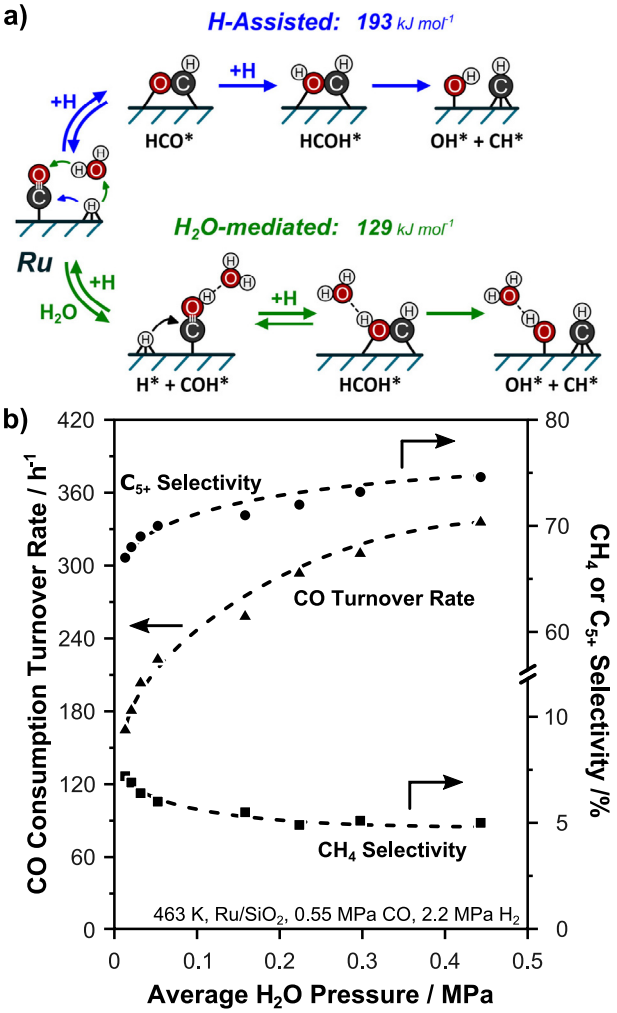

Fig. 5. (a) H-assisted CO activation can be further mediated by proton coupled electron transfer reactions that facilitate O—H bond formation and ultimately C—O cleavage via HCOH transition states. (b) CO turnover rates increase with increasing H_2O pressure as CH_4 selectivity decreases and the selectivity to $C_{\geq 5}$ species increases (463 K, 0.55 MPa CO, 2.2 MPa H_2, Ru/SiO_2) [73].

The intensity and frequency of CO* infrared stretches during FTS are not affected by changes in H_2O pressure (0–0.1 MPa) that led to 1.4-fold higher rates (473 K, $H_2/CO = 2$, 0.17 MPa CO, Co/SiO_2). These data indicate that H_2O did not detectably influence the coverage or type of CO*, remove unreactive residues that prevent CO* binding, or influence local CO concentrations by changing diffusion rates [17]. Any relevant H_2O-derived species must therefore act to increase the rates of kinetically relevant H-assisted CO* dissociation steps.

Fig. 5a depicts H-assisted CO* activation with and without H_2O-mediated O—H bond formation and their apparent activation barriers (referenced to a CO*-covered surface and the stoichiometric amounts of gaseous molecules required to form the TS, as in Rxn. (5)) on Ru_{201} nanoparticles models. H_2O-mediated routes have the lower energy barrier along the reaction coordinate and involve H* shuttling mediated by H_2O from a Ru-atom to the O-atom in the first H* addition to CO*, which forms COH* (bound through C-atom). H_2O interacts with COH* via H-bonding as the second H-addition forms *HCOH* and then dissociates to CH* and OH*. The simultaneous occurrence of these two paths, and the inclusion of a site-blocking term for H_2O leads to the rate equation:

$$r_{CO} = \frac{\alpha P_{H_2} P_{CO} + \gamma P_{H_2} P_{CO} P_{H_2O}}{\left(1 + K_{CO} P_{CO} + K_{H_2O} P_{H_2O}\right)^2} \tag{11}$$

by analogy with the one for anhydrous rates (Eq. (1)), where α is given for the anhydrous route in Eq. (1) and γ is a lumped rate constant for the H_2O-mediated pathway. Eq. (11) accurately describes the effects of H_2O pressure on measured turnover rates on Ru/SiO_2 catalysts (Fig. 5b) [73] and Co/SiO_2 [17] catalysts.

The effective enthalpy barriers for these two paths suggest that H_2O-assisted routes (corresponding to γ) are more facile (by 73 kJ mol^{-1}) than anhydrous routes (corresponding to α). Such enthalpic stabilization is compensated in part by entropy losses upon H_2O binding, thus making free energy barriers only slightly lower for H_2O-mediated than anhydrous routes (2 kJ mol^{-1} DFT; 8 kJ mol^{-1} from α and γ values from rate data), leading to parallel contributions to measured rates that are of similar magnitude (Fig. 5b).

The effects of H_2O on chain length reflect higher H_2O-derived monomer formation rates that cause each given chain to "find" more monomers before a termination event (H-addition, β-hydrogen elimination). Yet, catalysts and conditions that do not cause H_2O-induced rate enhancements still show H_2O-enhanced chain growth probabilities. This reflects how H_2O-derived species occupy a fraction of the surface, but enhance monomer formation rates on the rest, as discussed next; in doing so, the first effect leads to a decrease in the areal density

of growing chains. Monomers form via H-assisted CO activation (anhydrous or H_2O-mediated) predominantly in the immediate vicinity of growing chains, which disrupt the dense CO* adlayer. Consequently, monomer formation rates per chain are increased by H_2O, irrespective of the surface fraction occupied by CO* or H_2O-derived species; monomer formation, and thus FTS, turnover rates (based on exposed Co surfaces) depend, however, on the fraction of the surface that contains CO*.

5. A few chains grow fast because they locally disrupt dense CO* adlayers and create "space to form CH* monomers

The non-ideality of the dense CO* adlayers prevalent during FTS create an environment that allows chains to grow long and fast in an unexpected manner, a finding seemingly at odds with the formation of monomers uniformly throughout the adlayers, which would require their facile migration through a dense CO* adlayer to reach a few growing chains. ^{12}CO-^{13}CO isotopic transient experiments on Co and Fe catalysts determined the intramolecular location of ^{13}C-atoms within chains as the isotopic composition within the reactive CO pool evolved with time; the analysis of such data showed that only a few chains grow very fast at any one time during the transient [92]. The total ^{13}C content in such chains increased with time, as the reactive pool evolved from $^{12}CO^*$ to $^{13}CO^*$, but at each time the ^{13}C-content in each product was essentially identical at all C-positions along the alkene backbone, indicating that all C-atoms were added to a chain within a time when the ^{13}C-content in the monomer pool was essentially unchanged. Such an observation requires that monomers preferentially form in the immediate vicinity of the growing chain, to circumvent the need for rapid surface diffusion through dense CO* adlayers.

The formation of monomers next to a growing chain may simply reflect a role of CO*, the predominant surface species, as the monomer and its insertion into the M—C bonds in growing chains (often depicted as alkyls), as in alkyl migration routes ubiquitous in carbonylation by organometallic complexes [93,94]. Such routes would form oxygenates, detected as minority FTS products. FTS rates, however, reflect monomer formation rates and are proportional to H_2 pressure; these kinetic effects are not consistent with non-activated CO* as the predominant monomer. Monomers form instead, as discussed above, via H-assisted CO* dissociations that form CH* monomers. The formation of such monomers may benefit from the space created by chains that disrupt locally dense CO* adlayers; this environment may avoid the need for the endothermic desorption of a vicinal CO* to bind the *HCO–H*♯ transition states.

Carbene (CH_2^*) species as FTS monomers were inferred from the ability of diazomethane (CH_2N_2) to insert C-atoms from its CH_2^* decomposition fragment into chains during CO-H_2 reactions on Co catalysts at ambient pressures [8]. These CH_2^*-type species derived from an extraneous source were inserted into chains. The insertion of CH_2^* (or any CH_x^*) requires preceding CO* activation events through H-assisted routes that are also required to initiate chains; consequently, it seems implausible that similar steps can be so much faster for monomer formation than for the incipient formation of a growing chain, in contradiction with the conclusions from isotopic switching experiments [92].

Once again, the unusual environment created by dense CO* adlayers provides a mechanism by which a few chains can grow very rapidly without requiring monomer migration through crowded surfaces [44]. A theoretical assessment of such routes requires an analysis of the nature of such growing chains. On Ru_{218} half-particle models at 1.04 ML CO*, bound alkylidynes (RC*, CH* when R = H) are more stable than alkylidenes (RCH*, CH_2^*) or alkyls (RCH_2^*, CH_3^*; typically considered as chains); the free energies of formation of CH_2^* (81 kJ mol^{-1}; Rxn. (6); 500 K, 1 bar) and CH_3^* (18 kJ mol^{-1}; Rxn. (7)) from CH* and H* are positive:

$$CH^* + H^* \rightarrow CH_2^* \qquad \text{Rxn.(6)}$$

$$CH_2^* + H^* \rightarrow CH_3^* \qquad \text{Rxn.(7)}$$

These values would give CH* coverages at least 10^8-larger than either CH_2^* or CH_3^* (at 0.5–5 MPa H_2, 500 K); a similar preference for alkylidyne species is also evident for C_2–C_4 RCH_x^* species [44]. Thus, growing chains predominantly exist as alkylidynes [95,96] and not as the alkyls considered in carbene-mediated routes [6-9].

Such chains emerge via the formation of isolated CH* species within the CO* adlayer via H-assisted routes; these CH* species can (i) add H* to form CH_4; (ii) react with CO* to form C—C bonds (CO*-insertion); or (iii) form a C—C bond with another CH_x^* that forms nearby. The predominant use of monomers to form long chains (instead of CH_4 or oxygenates) supports the preferential formation of CH_x^* near alkylidyne chains; this preference is expected to become even stronger as CO* adlayers densify and the local disruptions become more consequential; as a result, fewer form at the undisrupted regions within CO* adlayers, where their reaction with H* would form CH_4 before they encounter a chain. Such processes account for the strong effects of CO pressure on CH_4 selectivity and product molecular weight, which cannot be described by Langmuirian chain growth models [44].

DFT-derived activation enthalpies and free energies (500 K, 1 bar) for H-assisted CO* dissociation on Ru_{218} models at 1.04 ML CO* are 98 and 15 kJ mol^{-1} lower on average, respectively, when these steps occur next to an alkylidyne chain instead of unperturbed CO* adlayers [44], indicative of the preferential formation of monomers near such chains. Chains form by desorbing one CO* ($-\Delta G_{ads,CO}$ = 22 kJ mol^{-1}, Fig. 6g) from a dense adlayer to create "space" for the H-assisted CO* activation TS; this TS decomposes to form CH* in a binding configuration that leaves a metal atom relatively exposed (Fig. 6a); CH_2^* and CH_3^* species, in contrast, coordinate more strongly and prevent the involvement of that metal atom in TS stabilization. The TS for activating another CO* next to a CH* "chain" forms without requiring the desorption of a CO* molecule or any significant distortions of the vicinal CO* adlayer because the TS and CH* can share a single metal atom (shown centrally in Fig. 6a and 6d) [44]. This is not the case for the formation of the same TS near CH_2^* or CH_3^* "chains", because CH_2^* or CH_3^* block the coordinating metal atom (Fig. 6e and 6f). The apparent free energy barrier for CO* activation (Eq. (9)) is 24 kJ mol^{-1} smaller next to a CH* than on the unperturbed adlayer; the differences in activation enthalpies are much larger (234 kJ mol^{-1} at the unperturbed adlayer; 127 kJ mol^{-1} next to CH*). These differences reflect the energetics of CO* desorption which has a ΔH of 104 kJ mol^{-1} and a ΔS of 164 J mol^{-1} K^{-1}, resulting in a ΔG of 22 kJ mol^{-1} (1 bar, 500 K). DFT-derived activation enthalpies (and free energies) for H-assisted CO activation steps are similar next to C_1-C_4 alkylidynes (CH*, CH_3C^*, $C_2H_5C^*$, $C_3H_7C^*$) with activation enthalpies ranging from 127 to 145 kJ mol^{-1} (and free energies from 204 to 220 kJ mol^{-1})—values which are, on average, 98 and 15 kJ mol^{-1} lower, respectively, than CO* dissociation on unperturbed adlayers. These monomer formation activation barriers at locations vicinal to growing alkylidyne chains

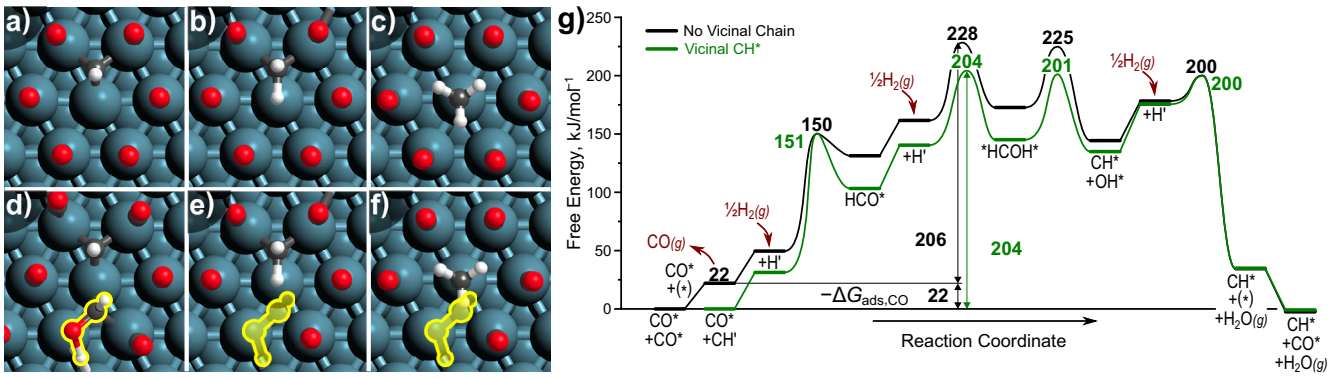

Fig. 6. (a-d) DFT-calculated structures of CH*, CH_2*, CH_3*, and the *HCO–H*≠ transition state vicinal to a CH*. (e-f) Overlays of the *HCO–H*≠ transition state and the structures of CH_2* and CH_3*. (g) Free energy diagrams for the H-assisted CO* activation without a vicinal chain (black) and the same reaction vicinal to a CH* (green) on Ru_{218} half-particle models at 1.044 ML CO* (500 K, 1 bar). Effective energy barriers to form transition states from a CO*-covered surface with or without a CH* 'chain' and stoichiometric amounts of gas species are shown for each transition state.

resemble those measured on Ru and Co catalysts [5,33,52-54]; the involvement H_2O-assisted routes at such locations and the presence of CO* adlayers denser than at the 1.04 ML CO* used in these DFT methods would give rise to even lower FTS activation barriers in practice.

The CH*–CH* reactions that consume monomers and lengthen chains involve small DFT-derived enthalpy barriers (88 kJ mol^{-1}), demonstrating that FTS rates are limited by the formation of monomers instead of their addition to chains. FTS product chains initiate slowly and rapidly grow because chains favor the formation of the CH* monomers in their immediate vicinity. As before, this realization emerges from the recognition of the essential role of dense CO* adlayers and the non-Langmuirian effects caused by coadsorbate repulsion on reactants and transition states.

6. A final perspective and a summary - dense CO* adlayers as enablers of Fischer-Tropsch synthesis turnovers

In this Perspective, the matter of whether defect site architectures or adlayer environments account for the enduring puzzles described here has sided with the latter, without ignoring that surface atom coordination matters, albeit in most cases to favor FTS turnovers on low-index Co and Ru surfaces. In doing so, our work has sought to rebalance a historical emphasis on concepts derived from stoichiometric binding and reactions of CO on sparsely covered extended surfaces with the reality of curved nanoparticles covered by dense CO* adlayers at the pressures required for FTS turnovers and chain growth. Such a balance and the role of CO* adlayers and H_2O "cocatalysts" (via proton-coupled electron transfer) as essential enablers of FTS turnovers have precluded the use of convenient Langmuirian constructs to describe the dynamics of surface catalysis.

The emergence of H-assisted and H_2O-assisted CO activation routes as the prevalent paradigm resolved the puzzling higher reactivity of low-index surfaces and the higher turnover rates measured on larger Co and Ru nanoparticles (Sections 2 and 4). The preeminence of bimolecular routes (over unassisted routes involving bare sites) in dissociating strong bonds on crowded surfaces has become the mechanistic norm for many other reactions. Dense adlayers weaken CO* binding through intermolecular repulsion. As a result, CO* becomes more reactive and easier to desorb, so as to create "space" for binding the TS for H-assisted CO* activation steps (Section 3). The discomfort created by these dense adlayers is felt by CO* more strongly than by the relevant TS, thus causing the preferential destabilization of the reactants over the kinetically relevant transition state. The disruption of such adlayers (by the incipient formation of a chain) allows such TS structures to form next to a chain without requiring CO* desorption to create additional space (Section 5). This, in turn, allows CH* monomers to react preferentially with chains and to circumvent the precarious formation of CH* within an undisrupted adlayer, from which they must migrate to add to chains with the intervening dangers of forming CH_4 via reactions with H*. The properties of dense adlayers are essential for fast FTS turnovers and high chain growth selectivity, but also for resolving those conundrums and puzzles that have persisted throughout the long and storied history of the Fischer-Tropsch synthesis.

Declaration of Competing Interest

The authors declare that they have no known competing financial interests or personal relationships that could have appeared to influence the work reported in this paper.

References

[1] E. Iglesia, S.C. Reyes, R.J. Madon, S.L. Soled, Selectivity control and catalyst design in the Fischer-Tropsch synthesis: sites, pellets, and reactors, in: Advances in Catalysis, Academic Press, 1993, pp. 221–302, https://doi.org/10.1016/S0360-0564(08)60579-9.
[2] F. Fischer, H. Tropsch, The synthesis of petroleum at atmospheric pressures from gasification products of coal, Brennstoff-Chemie. 7 (1926) 97–104.
[3] L.C. Browning, P.H. Emmett, Equilibrium Measurements in the Ni 3 C—Ni—CH 4 —H 2 and Co 2 C—Co—CH 4 —H 2 Systems, J. Am. Chem. Soc. 74 (7) (1952) 1680–1682.
[4] B.H. Davis, Fischer-Tropsch synthesis: current mechanism and futuristic needs, Fuel Process. Technol. 71 (1-3) (2001) 157–166, https://doi.org/10.1016/S0378-3820(01)00144-8.
[5] H.H. Storch, N. Golumbic, R.B. Anderson, The Fischer-Tropsch and Related Synthesis, Wiley, New York, 1951.
[6] P.M. Maitlis, A new view of the Fischer-Tropsch polymerisation reaction, Pure Appl. Chem. 61 (1989) 1747–1754, https://doi.org/10.1351/pac198961101747.
[7] R.C. Brady, R. Pettit, Reactions of diazomethane on transition-metal surfaces and their relationship to the mechanism of the Fischer-Tropsch reaction, J. Am. Chem. Soc. 102 (19) (1980) 6181–6182, https://doi.org/10.1021/ja00539a053.
[8] R.C. Brady, R. Pettit, On the mechanism of the Fischer-Tropsch reaction. The chain propagation step, J. Am. Chem. Soc. 103 (5) (1981) 1287–1289.

[9] L. Foppa, M. Iannuzzi, C. Copéret, A. Comas-Vives, Facile Fischer-Tropsch chain growth from CH2 monomers enabled by the dynamic CO adlayer, ACS Catal. 9 (7) (2019) 6571–6582, https://doi.org/10.1021/acscatal.9b00239.
[10] H.-Y. Su, Y. Zhao, J.-X. Liu, K. Sun, W.-X. Li, First-principles study of structure sensitivity of chain growth and selectivity in Fischer-Tropsch synthesis using HCP cobalt catalysts, Catal. Sci. Technol. 7 (14) (2017) 2967–2977, https://doi.org/10.1039/C7CY00706J.
[11] M. Zhuo, K.F. Tan, A. Borgna, M. Saeys, Density functional theory study of the CO insertion mechanism for Fischer–Tropsch synthesis over Co catalysts, J. Phys. Chem. C 113 (19) (2009) 8357–8365, https://doi.org/10.1021/jp900281h.
[12] B. Todic, W. Ma, G. Jacobs, B.H. Davis, D.B. Bukur, CO-insertion mechanism based kinetic model of the Fischer-Tropsch synthesis reaction over Re-promoted Co catalyst, Catal. Today 228 (2014) 32–39, https://doi.org/10.1016/j.cattod.2013.08.008.
[13] R.A. van Santen, A.J. Markvoort, Chain growth by CO insertion in the Fischer-Tropsch reaction, ChemCatChem 5 (11) (2013) 3384–3397, https://doi.org/10.1002/cctc.201300173.
[14] M. Zhuo, A. Borgna, M. Saeys, Effect of the CO coverage on the Fischer-Tropsch synthesis mechanism on cobalt catalysts, J. Catal. 297 (2013) 217–226, https://doi.org/10.1016/j.jcat.2012.10.008.
[15] L. Foppa, C. Copéret, A. Comas-Vives, Increased back-bonding explains step-edge reactivity and particle size effect for CO activation on Ru nanoparticles, J. Am. Chem. Soc. 138 (51) (2016) 16655–16668, https://doi.org/10.1021/jacs.6b08697.
[16] B.T. Loveless, C. Buda, M. Neurock, E. Iglesia, CO chemisorption and dissociation at high coverages during CO hydrogenation on Ru catalysts, J. Am. Chem. Soc. 135 (16) (2013) 6107–6121, https://doi.org/10.1021/ja311848e.
[17] S. Krishnamoorthy, M. Tu, M.P. Ojeda, D. Pinna, E. Iglesia, An investigation of the effects of water on rate and selectivity for the Fischer-Tropsch synthesis on cobalt-based catalysts, J. Catal. 211 (2) (2002) 422–433, https://doi.org/10.1006/jcat.2002.3749.
[18] J.P. den Breejen, P.B. Radstake, G.L. Bezemer, J.H. Bitter, V. Frøseth, A. Holmen, K.P. de Jong, On the origin of the cobalt particle size effects in Fischer-Tropsch catalysis, J. Am. Chem. Soc. 131 (20) (2009) 7197–7203, https://doi.org/10.1021/ja901006x.
[19] Q. Ge, M. Neurock, Adsorption and activation of CO over flat and stepped Co surfaces: a first principles analysis, J. Phys. Chem. B 110 (2006) 15368–15380, https://doi.org/10.1021/jp060477i.
[20] K. Høydalsvik, J.B. Fløystad, A. Voronov, G.J.B. Voss, M. Esmaeili, J. Kehres, H. Granlund, U. Vainio, J.W. Andreasen, M. Rønning, D.W. Breiby, Morphology changes of co catalyst nanoparticles at the onset of Fischer–Tropsch synthesis, J. Phys. Chem. C 118 (5) (2014) 2399–2407, https://doi.org/10.1021/jp4052193.
[21] R. Pestman, W. Chen, E. Hensen, New insight into the rate determining step and active sites in the Fischer-Tropsch reaction over cobalt catalysts, ACS Catal. 9 (5) (2019) 4189–4195, https://doi.org/10.1021/acscatal.9b00185.
[22] H. Oosterbeek, Bridging the pressure and material gap in heterogeneous catalysis: cobalt Fischer-Tropsch catalysts from surface science to industrial application, Phys. Chem. Chem. Phys. 9 (27) (2007) 3570–3576, https://doi.org/10.1039/B703003G.
[23] M.J. Kale, P. Christopher, Utilizing quantitative *in Situ* FTIR spectroscopy to identify well-coordinated Pt atoms as the active site for CO oxidation on Al_2O_3 -supported Pt catalysts, ACS Catal. 6 (2016) 5599–5609, https://doi.org/10.1021/acscatal.6b01128.
[24] J. Liu, D. Hibbitts, E. Iglesia, Dense CO adlayers as enablers of CO hydrogenation turnovers on Ru surfaces, J. Am. Chem. Soc. 139 (34) (2017) 11789–11802, https://doi.org/10.1021/jacs.7b04606.
[25] H. Ay, E. Iglesia, Effects of dense CO adlayers during CO hydrogenation on supported cobalt clusters, Unpublished. (n.d.).
[26] A. Tuxen, S. Carenco, M. Chintapalli, C.-H. Chuang, C. Escudero, E. Pach, P. Jiang, F. Borondics, B. Beberwyck, A.P. Alivisatos, G. Thornton, W.-F. Pong, J. Guo, R. Perez, F. Besenbacher, M. Salmeron, Size-dependent dissociation of carbon monoxide on cobalt nanoparticles, J. Am. Chem. Soc. 135 (6) (2013) 2273–2278, https://doi.org/10.1021/ja3105889.
[27] J.M.G. Carballo, J. Yang, A. Holmen, S. García-Rodríguez, S. Rojas, M. Ojeda, J.L.G. Fierro, Catalytic effects of ruthenium particle size on the Fischer-Tropsch Synthesis, J. Catal. 284 (1) (2011) 102–108, https://doi.org/10.1016/j.jcat.2011.09.008.
[28] N. Cant, A.T. Bell, Studies of carbon monoxide hydrogenation over ruthenium using transient response techniques, J. Catal. 73 (1982) 257–271.
[29] D. Hibbitts, E. Iglesia, Prevalence of bimolecular routes in the activation of diatomic molecules with strong chemical bonds (O_2, NO, CO, N_2) on catalytic surfaces, Acc. Chem. Res. 48 (5) (2015) 1254–1262, https://doi.org/10.1021/acs.accounts.5b00063.
[30] M. Ojeda, R. Nabar, A.U. Nilekar, A. Ishikawa, M. Mavrikakis, E. Iglesia, CO activation pathways and the mechanism of Fischer-Tropsch synthesis, J. Catal. 272 (2) (2010) 287–297, https://doi.org/10.1016/j.jcat.2010.04.012.
[31] E. Iglesia, Design, synthesis, and use of cobalt-based Fischer-Tropsch synthesis catalysts, Appl. Catal. A 161 (1-2) (1997) 59–78, https://doi.org/10.1016/S0926-860X(97)00186-5.
[32] R.S. Dixit, L.L. Tavlarides, Kinetics of the Fischer-Tropsch Synthesis, Ind. Eng. Chem. Process Des. Dev. 22 (1) (1983) 1–9.
[33] I.C. Yates, C.N. Satterfield, Intrinsic kinetics of the Fischer-Tropsch synthesis on a cobalt catalyst, Energy Fuels 5 (1) (1991) 168–173, https://doi.org/10.1021/ef00025a029.
[34] A.D. Allian, K. Takanabe, K.L. Fujdala, X. Hao, T.J. Truex, J. Cai, C. Buda, M. Neurock, E. Iglesia, Chemisorption of CO and mechanism of CO oxidation on supported platinum nanoclusters, J. Am. Chem. Soc. 133 (12) (2011) 4498–4517, https://doi.org/10.1021/ja110073u.
[35] C. Pedrero, T. Waku, E. Iglesia, Oxidation of CO in H2–CO mixtures catalyzed by platinum: alkali effects on rates and selectivity, J. Catal. 233 (1) (2005) 242–255, https://doi.org/10.1016/j.jcat.2005.04.005.
[36] J.P. Biberian, M.A. Van Hove, A new model for CO ordering at high coverages on low index metal surfaces: A correlation between leed, HREELS and IRS II. CO adsorbed on fcc (111) and hcp (0001) surfaces, Surf. Sci. Lett. 138 (2-3) (1984) A91, https://doi.org/10.1016/0167-2584(84)90378-5.
[37] H. Pfnür, D. Menzel, F.M. Hoffmann, A. Ortega, A.M. Bradshaw, High resolution vibrational spectroscopy of CO on Ru(001): the importance of lateral interactions, Surf. Sci. 93 (1980) 431–452.
[38] H. Pfnür, D. Menzel, The influence of adsorbate interactions on kinetics and equilibrium for CO on Ru(001). I. Adsorption kinetics, J. Chem. Phys. 79 (5) (1983) 2400–2410, https://doi.org/10.1063/1.446047.
[39] M.E. Bridge, C.M. Comrie, R.M. Lambert, Chemisorption studies on cobalt single crystal surfaces, Surf. Sci. 67 (2) (1977) 393–404.
[40] D.E. Starr, H. Bluhm, CO adsorption and dissociation on Ru(0001) at elevated pressures, Surf. Sci. 608 (2013) 241–248, https://doi.org/10.1016/j.susc.2012.10.014.
[41] F. Tao, S. Dag, L.-W. Wang, Z. Liu, D.R. Butcher, H. Bluhm, M. Salmeron, G.A. Somorjai, Break-up of stepped platinum catalyst surfaces by high CO coverage, Science 327 (5967) (2010) 850–853, https://doi.org/10.1126/science:1182122.
[42] S. Shetty, R.A. van Santen, CO dissociation on Ru and Co surfaces: The initial step in the Fischer-Tropsch synthesis, Catal. Today 171 (1) (2011) 168–173, https://doi.org/10.1016/j.cattod.2011.04.006.
[43] A. Comas-Vives, K. Furman, D. Gajan, M.C. Akatay, A. Lesage, F.H. Ribeiro, C. Copéret, Predictive morphology, stoichiometry and structure of surface species in supported Ru nanoparticles under H2 and CO atmospheres from combined experimental and DFT studies, Phys. Chem. Chem. Phys. 18 (3) (2016) 1969–1979, https://doi.org/10.1039/C5CP06710C.
[44] D.D. Hibbitts, E. Dybeck, T. Lawlor, M. Neurock, E. Iglesia, Preferential activation of CO near hydrocarbon chains during Fischer-Tropsch synthesis on Ru, J. Catal. 337 (2016) 91–101, https://doi.org/10.1016/j.jcat.2016.01.010.
[45] P. Kravchenko, V. Krishnan, D. Hibbitts, Mechanism and effects of coverage and particle morphology on Rh-catalyzed NO–H_2 reactions, J. Phys. Chem. C 124 (24) (2020) 13291–13303, https://doi.org/10.1021/acs.jpcc.0c04024.
[46] A.S. Almithn, D.D. Hibbitts, Supra-monolayer coverages on small metal clusters and their effects on H_2 chemisorption particle size estimates, AIChE J. 64 (8) (2018) 3109–3120, https://doi.org/10.1002/aic.v64.8.
[47] A. Almithn, D. Hibbitts, Effects of catalyst model and high adsorbate coverages in ab initio studies of alkane hydrogenolysis, ACS Catal. 8 (7) (2018) 6375–6387, https://doi.org/10.1021/acscatal.8b01114.
[48] E. Yik, D. Hibbitts, H. Wang, E. Iglesia, Hydrogenation and C-S bond activation pathways in thiophene and tetrahydrothiophene reactions on sulfur-passivated surfaces of Ru, Pt, and Re nanoparticles, Appl. Catal. B 291 (2021) 119797, https://doi.org/10.1016/j.apcatb.2020.119797.
[49] R.K. Brandt, R.S. Sorbello, R.G. Greenler, Site-specific, coupled-harmonic-oscillator model of carbon monoxide adsorbed on extended, single-crystal surfaces and on small crystals of platinum, Surf. Sci. 271 (3) (1992) 605–615.
[50] B. Hammer, L.B. Hansen, J.K. Nørskov, Improved adsorption energetics within density-functional theory using revised Perdew-Burke-Ernzerhof functionals, Phys. Rev. B. 59 (11) (1999) 7413–7421, https://doi.org/10.1103/PhysRevB.59.7413.
[51] I.M. Ciobica, R.A. van Santen, Carbon monoxide dissociation on planar and stepped ru(0001) surfaces, J. Phys. Chem. B 107 (16) (2003) 3808–3812, https://doi.org/10.1021/jp030010x.
[52] E.J. Gibson, C.C. Hall, The Fischer-Tropsch synthesis with cobalt catalysts: the effect of process conditions on the composition of the reaction products, J. Appl. Chem. 4 (1954) 49–61.
[53] R.B. Anderson, Catalysts for the Fischer-Tropsch synthesis, Catalysis. 4 (1956) 29–255.

[54] F. Fischer, H. Pichler, The synthesis of paraffin from carbon monoxide and hydrogen upon cobalt catalysts (medium pressure synthesis), Brennst.-Chem. 20 (1939) 41–48.
[55] S. Shetty, R.A. van Santen, Hydrogen induced CO activation on open Ru and Co surfaces, Phys. Chem. Chem. Phys. 12 (2010) 6330–6332, https://doi.org/10.1039/b926731j.
[56] T. Zubkov, G.A. Morgan, J.T. Yates, O. Kühlert, M. Lisowski, R. Schillinger, D. Fick, H.J. Jänsch, The effect of atomic steps on adsorption and desorption of CO on Ru(109), Surf. Sci. 526 (1-2) (2003) 57–71, https://doi.org/10.1016/S0039-6028(02)02655-9.
[57] W. Chen, B. Zijlstra, I.A.W. Filot, R. Pestman, E.J.M. Hensen, Mechanism of carbon monoxide dissociation on a cobalt Fischer-Tropsch catalyst, ChemCatChem 10 (1) (2018) 136–140, https://doi.org/10.1002/cctc.201701203.
[58] N.M. Wilson, D.W. Flaherty, Mechanism for the direct synthesis of H2O2 on Pd clusters: heterolytic reaction pathways at the liquid-solid interface, J. Am. Chem. Soc. 138 (2) (2016) 574–586, https://doi.org/10.1021/jacs.5b10669.
[59] B.N. Zope, D.D. Hibbitts, M. Neurock, R.J. Davis, Reactivity of the gold/water interface during selective oxidation catalysis, Science 330 (6000) (2010) 74–78, https://doi.org/10.1126/science:1195055.
[60] D.D. Hibbitts, M. Neurock, Influence of oxygen and pH on the selective oxidation of ethanol on Pd catalysts, J. Catal. 299 (2013) 261–271, https://doi.org/10.1016/j.jcat.2012.11.016.
[61] M. Ojeda, B.-Z. Zhan, E. Iglesia, Mechanistic interpretation of CO oxidation turnover rates on supported Au clusters, J. Catal. 285 (1) (2012) 92–102, https://doi.org/10.1016/j.jcat.2011.09.015.
[62] D.D. Hibbitts, R. Jiménez, M. Yoshimura, B. Weiss, E. Iglesia, Catalytic NO activation and NO–H_2 reaction pathways, J. Catal. 319 (2014) 95–109, https://doi.org/10.1016/j.jcat.2014.07.012.
[63] G. Blyholder, M. Lawless, Hydrogen-assisted dissociation of CO on a catalyst surface, Langmuir 7 (1990) 140–141.
[64] W.K. Hall, R.J. Kokes, P.H. Emmett, Mechanism studies of the Fischer-Tropsch synthesis: the incorporation of radioactive ethylene, propionaldehyde and propanol, J. Am. Chem. Soc. 82 (5) (1960) 1027–1037, https://doi.org/10.1021/ja01490a005.
[65] G.P. van der Laan, A.A.C.M. Beenackers, Intrinsic kinetics of the gas–solid Fischer-Tropsch and water gas shift reactions over a precipitated iron catalyst, Appl Catal A Gen. 193 (1-2) (2000) 39–53.
[66] M. Ojeda, A. Li, R. Nabar, A.U. Nilekar, M. Mavrikakis, E. Iglesia, Kinetically relevant steps and h_2 /d_2 isotope effects in Fischer–Tropsch synthesis on FE and CO catalysts, J. Phys. Chem. C 114 (46) (2010) 19761–19770, https://doi.org/10.1021/jp1073076.
[67] L. Foppa, M. Iannuzzi, C. Copéret, A. Comas-Vives, CO methanation on ruthenium flat and stepped surfaces: Key role of H-transfers and entropy revealed by ab initio molecular dynamics, J. Catal. 371 (2019) 270–275, https://doi.org/10.1016/j.jcat.2019.02.008.
[68] D. Shi, J. Faria, T.N. Pham, D.E. Resasco, Enhanced activity and selectivity of fischer–tropsch synthesis catalysts in water/oil emulsions, ACS Catal. 4 (6) (2014) 1944–1952, https://doi.org/10.1021/cs500040n.
[69] E. Rytter, A. Holmen, Consorted vinylene mechanism for cobalt Fischer-Tropsch synthesis encompassing water or hydroxyl assisted CO-activation, Top. Catal. 61 (9-11) (2018) 1024–1034, https://doi.org/10.1007/s11244-018-0932-3.
[70] G.T.K.K. Gunasooriya, A.P. van Bavel, H.P.C.E. Kuipers, M. Saeys, Key role of surface hydroxyl groups in C-O activation during Fischer-Tropsch synthesis, ACS Catal. 6 (6) (2016) 3660–3664, https://doi.org/10.1021/acscatal.6b0063410.1021/acscatal.6b00634.s001.
[71] F. Romero-Sarria, L.F. Bobadilla, E.M. Jiménez Barrera, J.A. Odriozola, Experimental evidence of HCO species as intermediate in the Fischer tropsch reaction using operando techniques, Appl. Catal. B 272 (2020) 119032, https://doi.org/10.1016/j.apcatb.2020.119032.
[72] O.R. Inderwildi, S.J. Jenkins, D.A. King, Fischer–Tropsch mechanism revisited: alternative pathways for the production of higher hydrocarbons from synthesis gas, J. Phys. Chem. C 112 (2008) 1305–1307, https://doi.org/10.1021/jp710674q.
[73] D.D. Hibbitts, B.T. Loveless, M. Neurock, E. Iglesia, Mechanistic role of water on the rate and selectivity of Fischer-Tropsch synthesis on ruthenium catalysts, Angew. Chem. Int. Ed. 52 (47) (2013) 12273–12278, https://doi.org/10.1002/anie.201304610.
[74] M.G. Evans, M. Polanyi, Some applications of the transition state method to the calculation of reaction velocities, especially in solution, Trans. Faraday Soc. 31 (1935) 875, https://doi.org/10.1039/tf9353100875.
[75] R. Van Eldik, T. Asano, W.J. Le Noble, Activation and reaction volumes in solution. 2, Chem. Rev. 89 (3) (1989) 549–688, https://doi.org/10.1021/cr00093a005.
[76] R.A. Grieger, C.A. Eckert, Solvent effects on the activation volume of a Diels-Alder reaction, Trans. Faraday Soc. 66 (1970) 2579–2584, https://doi.org/10.1039/tf9706602579.
[77] G.A. Lawrance, D.R. Stranks, Role of activation volume in the elucidation of reaction mechanisms in octahedral coordination complexes, Acc. Chem. Res. 12 (11) (1979) 403–409, https://doi.org/10.1021/ar50143a004.
[78] F.-G. Klaerner, B. Krawczyk, V. Ruster, U.K. Deiters, Evidence for pericyclic and stepwise processes in the cyclodimerization of chloroprene and 1,3-butadiene from pressure dependence and stereochemistry. experimental and theoretical volumes of activation and reaction, J. Am. Chem. Soc. 116 (17) (1994) 7646–7657, https://doi.org/10.1021/ja00096a023.
[79] C.J. Kim, Water Addition for Increased CO/H2 Hydrocarbon Synthesis Activity Over Catalysts Comprising Cobalt, Ruthenium and Mixtures Thereof Which May Include a Promoter Metal, US patent 5,227,407, 1992 Mar 11.
[80] H. Schulz, E. vein Steen, M. Claeys, Selectivity and mechanism of Fischer-Tropsch synthesis with iron and cobalt catalysts, in: Natural Gas Conversion II - Proceedings of the Third Natural Gas Conversion Symposium, Elsevier, 1994: pp. 455–460. https://doi.org/10.1016/S0167-2991(08)63911-7
[81] T.K. Das, W.A. Conner, J. Li, G. Jacobs, M.E. Dry, B.H. Davis, Fischer–tropsch synthesis: kinetics and effect of water for a co/sio_2 catalyst, Energy Fuels 19 (2005) 1430–1439, https://doi.org/10.1021/ef049869j.
[82] S. Storsater, O. Borg, E. Blekkan, A. Holmen, Study of the effect of water on Fischer-Tropsch synthesis over supported cobalt catalysts, J. Catal. 231 (2) (2005) 405–419, https://doi.org/10.1016/j.jcat.2005.01.036.
[83] S. Storsæter, Ø. Borg, E.A. Blekkan, B. Tøtdal, A. Holmen, Fischer-Tropsch synthesis over Re-promoted Co supported on Al_2O_3, SiO_2 and TiO_2: Effect of water, Catal. Today 100 (3-4) (2005) 343–347, https://doi.org/10.1016/j.cattod.2004.09.068.
[84] A.M. Hilmen, D. Schanke, K.F. Hanssen, A. Holmen, Study of the effect of water on alumina supported cobalt Fischer-Tropsch catalysts, Appl. Catal. A 186 (1-2) (1999) 169–188, https://doi.org/10.1016/S0926-860X(99)00171-4.
[85] A.K. Dalai, T.K. Das, K.V. Chaudhari, G. Jacobs, B.H. Davis, Fischer-Tropsch synthesis: Water effects on Co supported on narrow and wide-pore silica, Appl. Catal. A 289 (2) (2005) 135–142, https://doi.org/10.1016/j.apcata.2005.04.045.
[86] P.J. van Berge, J. van de Loosdrecht, S. Barradas, A.M. van der Kraan, Oxidation of cobalt based Fischer-Tropsch catalysts as a deactivation mechanism, Catal. Today 58 (4) (2000) 321–334, https://doi.org/10.1016/S0920-5861(00)00265-0.
[87] H. Schulz, M. Claeys, S. Harms, Effect of water partial pressure on steady state Fischer-Tropsch activity and selectivity of a promoted cobalt catalyst, in: Natural Gas Conversion IV, Elsevier, 1997, pp. 193–200. https://doi.org/10.1016/S0167-2991(97)80334-5.
[88] E. Rytter, Ø. Borg, N.E. Tsakoumis, A. Holmen, Water as key to activity and selectivity in Co Fischer-Tropsch synthesis: γ-alumina based structure-performance relationships, J. Catal. 365 (2018) 334–343, https://doi.org/10.1016/j.jcat.2018.07.003.
[89] K.D. Papavasileiou, Z.A. Makrodimitri, L.D. Peristeras, J. Chen, G.P. van der Laan, I. Rudra, A. Kalantar, I.G. Economou, Molecular simulation of*n* -octacosane–water mixture in titania nanopores at elevated temperature and pressure, J. Phys. Chem. C 120 (43) (2016) 24743–24753, https://doi.org/10.1021/acs.jpcc.6b07226.
[90] Q. Zheng, J.L. Brown, M.D. Mantle, A.J. Sederman, T.A. Baart, C.M. Guédon, L.F. Gladden, Water-wax behaviour in porous silica at low temperature Fischer-Tropsch conditions, Appl. Catal. A 572 (2019) 142–150, https://doi.org/10.1016/j.apcata.2018.11.022.
[91] M. Lualdi, G. Di Carlo, S. Lögdberg, S. Järås, M. Boutonnet, V. La Parola, L.F. Liotta, G.M. Ingo, A.M. Venezia, Effect of Ti and Al addition via direct synthesis to SBA-15 as support for cobalt based Fischer-Tropsch catalysts, Appl. Catal. A 443–444 (2012) 76–86, https://doi.org/10.1016/j.apcata.2012.07.026.
[92] C.A. Mims, L.E. McCandlish, Evidence for rapid chain growth in the Fischer-Tropsch synthesis over iron and cobalt catalysts, J. Phys. Chem. 91 (4) (1987) 929–937, https://doi.org/10.1021/j100288a033.
[93] J.-A. Andersen, J.R. Moss, Synthesis of an extensive series of manganese pentacarbonyl alkyl and acyl compounds: carbonylation and decarbonylation studies on [mn(r)(co)5] and [mn(cor)(co)5], Organometallics 13 (12) (1994) 5013–5020, https://doi.org/10.1021/om00024a051.
[94] H. Berke, R. Hoffmann, Organometallic migration reactions, J. Am. Chem. Soc. 100 (23) (1978) 7224–7236.
[95] I.M. Ciobîcă, G.J. Kramer, Q. Ge, M. Neurock, R.A. van Santen, Mechanisms for chain growth in Fischer-Tropsch synthesis over Ru(0001), J. Catal. 212 (2) (2002) 136–144, https://doi.org/10.1006/jcat.2002.3742.
[96] J. Cheng, P. Hu, P. Ellis, S. French, G. Kelly, C.M. Lok, Chain growth Mechanism in Fischer–Tropsch synthesis: A DFT study of C–C coupling over Ru, Fe, Rh, and Re surfaces, J. Phys. Chem. C 112 (2008) 6082–6086, https://doi.org/10.1021/jp711051e.